Optics Letters

Noninvasive, *in vivo* imaging of subcortical mouse brain regions with 1.7 μm optical coherence tomography

SHAU POH CHONG,[1] CONRAD W. MERKLE,[1] DYLAN F. COOKE,[2] TINGWEI ZHANG,[1] HARSHA RADHAKRISHNAN,[1] LEAH KRUBITZER,[2] AND VIVEK J. SRINIVASAN[1,*]

[1]Biomedical Engineering Department, University of California Davis, Davis, California 95616, USA
[2]Department of Psychology & Center for Neuroscience, University of California Davis, Davis, California 95616, USA
*Corresponding author: vjsriniv@ucdavis.edu

A spectral/Fourier domain optical coherence tomography (OCT) intravital microscope using a supercontinuum light source at 1.7 μm was developed to study subcortical structures noninvasively in the living mouse brain. The benefits of 1.7 μm for deep tissue brain imaging are demonstrated by quantitatively comparing OCT signal attenuation characteristics of cortical tissue across visible and near-infrared wavelengths. Imaging of hippocampal tissue architecture and white matter microvasculature are demonstrated *in vivo* through thinned-skull, glass coverslip-reinforced cranial windows in mice. Applications of this novel platform include monitoring disease progression and pathophysiology in rodent models of Alzheimer's disease and subcortical dementias, including vascular dementia.   © 2015 Optical Society of America

Two-photon fluorescence microscopy (2PM) [1] has significantly advanced neuroscience research over the past two decades by enabling visualization of cellular and vascular morphology and physiology beneath the surface of the living brain, particularly in rodents. However, deep cortical layers and subcortical brain regions remain beyond the reach of a typical two-photon fluorescence microscope, which operates at excitation wavelengths of ∼800 nm and achieves penetration depths of <600 μm. While amplified, higher pulse energy systems can achieve penetration depths of up to 1 mm [2]; further improvements at ∼800 nm excitation are mainly limited by scattering of excitation light and out-of-focus background fluorescence generated near the surface [3] while focusing deep. Recently, optical coherence tomography (OCT), along with associated Doppler and angiographic techniques, has emerged as a complementary method to two-photon microscopy. Though lacking the cellular and molecular specificity of 2PM, OCT is a label-free technique, achieves comparable imaging depths to 2PM, enables deep imaging with a lower NA than 2PM, performs volumetric imaging more rapidly than 2PM, and images through the intact [4] or thinned [5] skull in mouse models.

As scattering at 800 nm limits imaging depth and biological tissue scattering decreases with wavelength [6], recent efforts have investigated longer wavelengths in the 1–1.3 μm range for OCT [7] and 2PM [8] in the brain. While increasing the excitation wavelength beyond 1.3 μm further reduces scattering, this benefit is potentially mitigated by increased water absorption. Recently, excitation wavelengths in the 1.7 μm water absorption spectral window were shown to optimally deliver light to a focal plane deep in brain tissue, when attenuation due to both single scattering and absorption was accounted for [9]. Accordingly, subcortical penetration depths were achieved with third-harmonic generation and three-photon excited fluorescence in the mouse brain [9]. While longer wavelengths can focus deeper in scattering tissue, in OCT, unlike 2PM and 3PM, backscattering is the main source of contrast. Hence, increasing the wavelength may also reduce the useful backscattering signal. Prior OCT approaches in the 1.7 μm wavelength range include time-domain OCT systems using supercontinuum light sources [10], swept source OCT systems [11], and spectral domain OCT systems [12]. Improved OCT penetration depths in low water-content, highly scattering samples were shown at 1.7 μm, compared to 800 nm and 1.3 μm [13]. However, unlike these samples, the rodent brain has a water content of >70% [14], and deeper cortical and subcortical regions rich in lipids (myelin), possessing an absorption peak around 1.7 μm. Thus, the benefits of 1.7 μm OCT for deep imaging in biological tissue such as the brain remain unknown.

Here, we describe the design and implementation of a 1.7 μm spectral/Fourier domain OCT intravital microscope. Based on comparing OCT signal attenuation versus depth at a range of different wavelengths, we quantitatively show the benefits of 1.7 μm for deep brain imaging. We show that when

1.7 μm OCT images are appropriately compounded, white matter microvasculature and hippocampal tissue architecture are clearly visualized noninvasively in the mouse brain *in vivo*.

The 1.7 μm OCT system (Fig. 1A) used an unpolarized supercontinuum light source (SuperK EXW-12, NKT Photonics). The output beam was attenuated, spectrally filtered, and coupled to an SMF-28 fiber patch cord. The spectral range was centered at 1.7 μm with a 170 nm full-width at half-maximum (FWHM) bandwidth, which provided a theoretical axial resolution of 7.5 μm in air (5.6 μm in tissue, not accounting for shaping due to water absorption). The OCT setup used a customized wide-bandwidth 50/50 coupler with SMF-28 fiber. In the sample arm, the beam was collimated, raster scanned by a 2D galvanometer scanner (6210H, Cambridge Technology), and expanded 1.5× by a lens pair in a Keplerian configuration before being focused by a 5× objective (LSM03, Thorlabs, Inc.) with 36 mm focal length, resulting in a focused spot size of ∼15 μm FWHM at the focal plane. The reference arm contained a variable neutral density filter to adjust the reference power and a prism pair to compensate the dispersion caused by optics in the sample arm. The backscattered or backreflected beams from both arms were combined by the custom coupler and directed to a custom spectrometer. The output from the fiber was collimated using another 75 mm achromatic doublet. A volume transmission grating (600 lpmm, Wasatch Photonics), a focusing lens (150 mm achromatic doublet pair), and an extended InGaAs line-scan camera (SU-LDH-2.2, Sensors Unlimited) were used in the spectrometer. The spectral response of the extended InGaAs line-scan camera spanned from 0.9–2.2 μm with an acquisition window of 1024 pixels and maximum line rate of ∼47 kHz. The spectrum measured by the custom spectrometer was calibrated [15] and correlated against that measured by an optical spectrum analyzer (Fig. 1B). The calibrated spectral sampling interval was 0.24 nm, which provided an imaging depth of 3.05 mm in air, with a sensitivity roll-off of ∼10 dB over the first 2.5 mm (Fig. 1C). The camera was connected to a frame grabber (PCIe-1427, National Instruments, Austin, Texas), triggered by a NI 6363 digital I/O board (National Instruments, Austin, Texas), which also synchronously drove the 2D galvanometer scanner. The acquisition was controlled by a custom LabVIEW program that allowed various scanning patterns and fields of view.

Adult wild-type mice (male, 24–29 g C57BL/6 mice, $N = 3$, Charles River Lab, Massachusetts, USA) were used. The mouse was anesthetized with isoflurane with a gas mixture of 80% air and 20% oxygen. Artificial teardrops were applied to the eyes to prevent corneal dehydration. The mouse was then immobilized on a stereotactic frame (Stoelting Co., Illinois, USA) and a thinned-skull cranial window [16] for imaging was created over the parietal cortex. Prior to imaging, an additional custom-made head mount was fixed to reduce motion artifacts due to breathing. All experimental procedures and protocols were approved by the UC Davis Institutional Animal Care and Use Committee.

To determine the wavelength dependence of OCT attenuation in cortical tissue, the same location in a single mouse brain was imaged *in vivo* using multiple OCT systems in our laboratory (same day as window preparation), as shown in Figs. 2A–2C. Details about the visible OCT and 1.3 μm OCT can be found in our previous publications [17,18]. Briefly, the transverse resolutions ranged from 22 μm for visible OCT to 15 μm for 1.3 and 1.7 μm OCT, with sensitivity >90 dB for all systems. The incident powers on the sample were 5, 6, and 5 mW for visible OCT, 1.3 μm OCT, and 1.7 μm OCT, respectively. The respective line rates were 90, 91, and 40 kHz. Furthermore, both the 1.3 and 1.7 μm OCT employed the same objective lens. The focal plane was set near the surface of the cortex and the same location was imaged on each system. Before determining attenuation coefficients, the background offset and sensitivity roll-off were individually corrected for each system. Attenuation coefficients include effects of both tissue scattering and absorption (mainly water in the infrared and hemoglobin in the visible, as shown in Fig. 2D). The OCT signal versus depth was fit using an exponential decay model, $A \exp(-\mu_t z)$, over the first 200 μm, to determine the attenuation coefficient μ_t [19], presented in Fig. 2E. For low NAs, in the single scattering limit, $\mu_t = \mu_a + \mu_s$; however, accounting for multiple scattering, $\mu_t = \mu_a + a(g) * \mu_s$, where μ_a and μ_s are absorption and scattering coefficients, respectively, and $a(g)$ is a term dependent on anisotropy g [20]. Tissue scattering follows a power law relationship with wavelength, $\mu_s \sim \lambda^{-b}$, in which $1 < b < 2$ for most biological tissues [6]. The estimated attenuation coefficients in Fig. 2F are consistent with literature values [6]. In accordance with these results, paired *t*-tests, corrected for multiple comparisons (Fig. 2F), confirmed that 1.7 μm OCT had the smallest attenuation coefficient and visible OCT had the largest attenuation coefficient. Additionally, a younger mouse had a significantly lower attenuation coefficient than an older mouse ($p < 0.05$ using unpaired *t*-test), most likely due to increased myelination and scattering with age (Fig. 2G).

In Fig. 3A, a maximum intensity projection of a series of 20 cross-sectional images, with the focus placed around the corpus
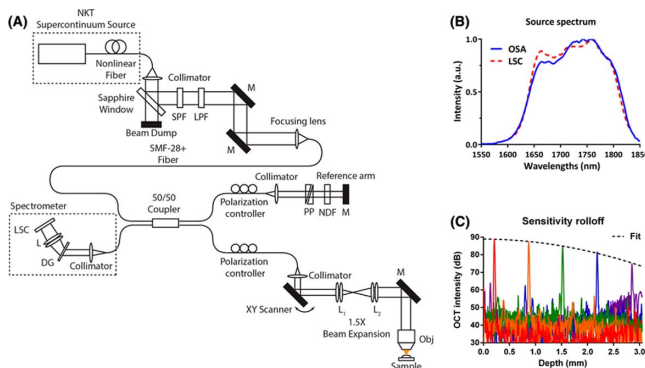
Fig. 1. (A) 1.7 μm OCT intravital microscope. The NKT supercontinuum light source was filtered by a short-pass filter (SPF) and a long-pass filter (LPF) after 7% reflection by a sapphire window before fiber coupling. M, mirror; PP, prism pair; NDF, neutral density filter; L, lens; DG, diffraction grating; LSC, line-scan camera; OBJ, objective lens. (B) Spectra measured either using a Fourier transform optical spectrum analyzer (blue solid line, OSA) or using our custom-made spectrometer (red-dotted line, LSC) agree. The FWHM bandwidths were almost identical, ∼170 nm, yielding a theoretical axial resolution of ∼7.5 μm in air (∼5.6 μm in tissue), though shaping due to water absorption will reduce the resolution *in vivo*. The total spectral range of our spectrometer was ∼246 nm. (C) The sensitivity roll-off of the system was approximately 10 dB over ∼2.5 mm in air (dotted line shows parabolic fit on a log scale).
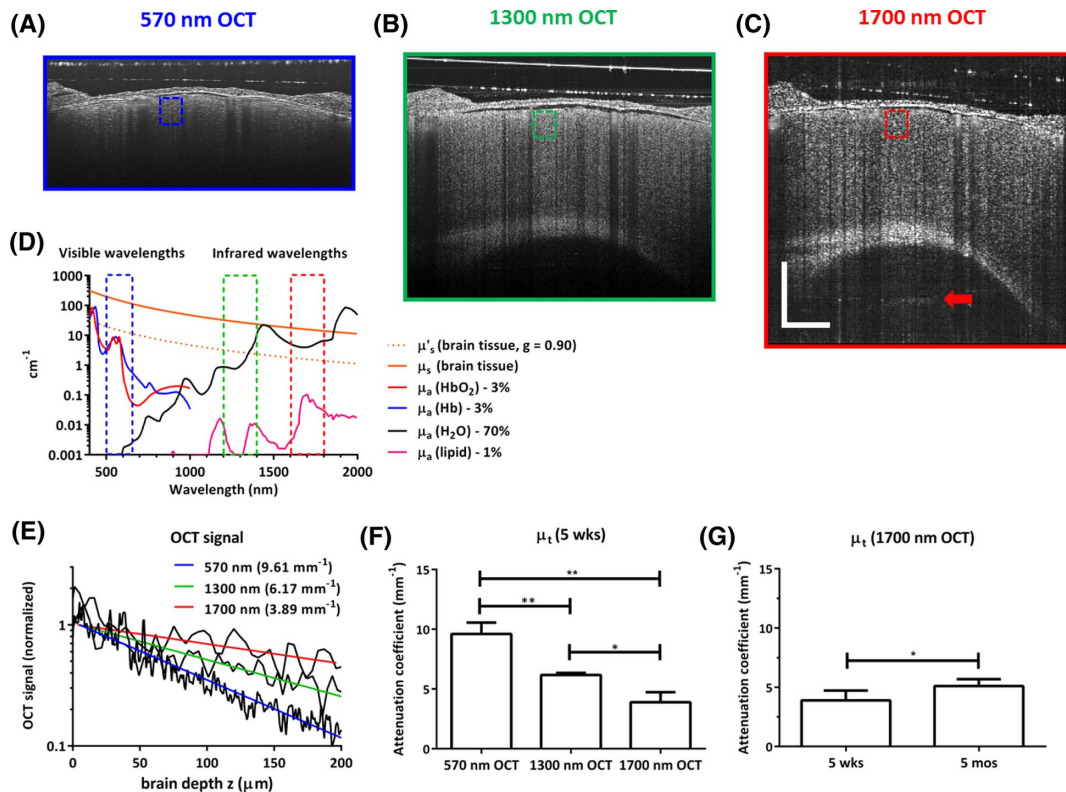
Fig. 2. *In vivo* imaging of the mouse brain through a thinned-skull cranial window was performed by visible (A), 1.3 μm (B), and 1.7 μm (C) OCT, by placing the focus at the cortical surface. Scale bars in (C) represent 0.5 mm and apply for all images, and the full axial imaging range for each system is displayed. Subcortical backscattering is only noted at 1700 nm (C, red arrow). Rostral is right and dorsal is up. (D) Absorption and scattering spectra of relevant brain tissue constituents, with dashed boxes showing wavelengths ranges for (A)–(C). (E) The attenuation of the OCT signal was determined using a simple exponential fit, $A\exp(-\mu_t z)$, where z is the imaging depth, over the first 200 μm of cortical tissue [boxes in (A)–(C)]. (F) Comparison of attenuation coefficients, measured at multiple coregistered locations in the same brain, shows that the 1.7 μm OCT attenuation coefficient was significantly lower than the attenuation coefficients at the other wavelengths ($*p < 0.05$, $**p < 0.01$, paired t-test). (G) A young mouse (5 weeks) had a lower attenuation coefficient ($*p < 0.05$, unpaired t-test) than an older mouse (5 months), most likely due to increased myelination and scattering with age.

callosum (cc), is shown. Layers or strata in the hippocampus proper are clearly visible through the thinned skull *in vivo* using 1.7 μm OCT. Figure 3B shows the outlines of the anatomical structures derived from photomicrographs of coregistered Nissl (C) and myelin-stained (D) tissue [21] from the same brain that was imaged. In particular, the corpus callosum (cc, green arrow) shows high reflectivity due to the high degree of myelination in white matter [22]. The stratum pyramidale (Py, blue arrow)

contains the cell bodies of the pyramidal neurons and thus appears as a low scattering band. On the other hand, the stratum lacunosum-moleculare (LMol, red arrow) contains Schaffer collateral fibers and perforant path fibers [23], which might explain the observed hyper-reflectivity.

The achievable penetration depth is highly dependent on the age, imaging location, and vascular patterns in individual mice. The mouse in Fig. 4A demonstrates more consistent
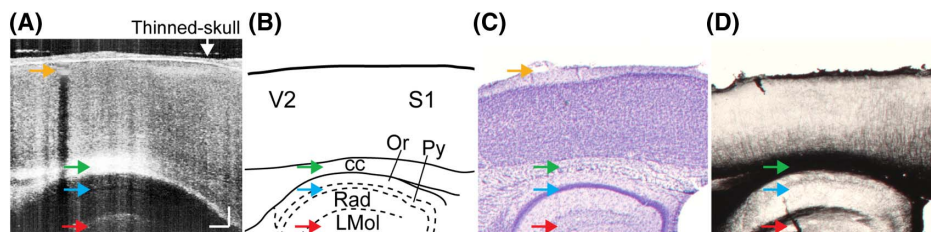
Fig. 3. *In vivo* imaging of subcortical regions through the thinned skull was achieved by deep focusing using 1.7 μm OCT. (A) A maximum intensity projection of a series of cross-sectional images shows subcortical structures, including the hippocampus. Multiple subcortical layers can be distinguished, with corresponding layers highlighted with blue and red arrows. Green arrows show the corpus callosum. Orange arrows mark a blood vessel visible in (A) and (C). (B) Outlines of corresponding anatomical structures derived from photomicrographs of Nissl (C) and myelin-stained (D) tissue from the same brain that was imaged. Divisions of the hippocampus are dashed. cc, corpus callosum; Or, stratum oriens; Py, stratum pyramidale; Rad, stratum radiatum; and LMol, stratum lacunosum-moleculare. Scale bar: 0.2 mm. Rostral is right and dorsal is up.
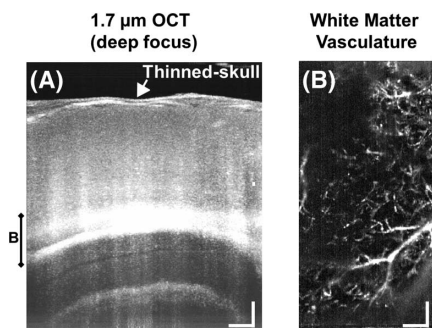
Fig. 4. *In vivo* imaging of subcortical regions noninvasively through the thinned skull was achieved by deep focusing using 1.7 μm OCT. (A) A maximum intensity projection of a series of cross-sectional images shows subcortical structures, including the hippocampus proper. (B) Microvasculature in deep white matter regions is visualized using an OCT angiography method and a maximum intensity projection. Scale bars: 0.2 mm.

hippocampal image quality than Fig. 3A, likely due to the lack of shadows from superficial vasculature. In this mouse, white matter microvasculature could be visualized using OCT angiography [4] at 1.7 μm (Fig. 4B).

When transitioning from 1.3 to 1.7 μm, scattering is reduced while absorption is increased (Fig. 2D). Single, nonforward scattering events cause pure signal attenuation [9], similar to absorption. However, detection of multiply scattered photons degrades signal localization and contrast [24]. Wavefront distortion [25] prevents deep focusing. The scattering coefficient of brain tissue is >40% lower at 1.7 μm compared to 1.3 μm in the literature [26], and our measured attenuation coefficient was ~37% lower at 1.7 μm compared to 1.3 μm (Fig. 2F), in spite of the higher absorption. OCT around 1.7 μm may also suffer less from multiple scattering, leading to better image contrast and spatial resolution at larger depths. Put another way, the signal penalty due to reduced backscattering, more lossy components, higher camera noise, and increased water absorption at 1.7 μm can easily be compensated by longer integration times, more averaging, or higher sample powers. On the other hand, a loss in image contrast and resolution, or "blur," due to multiple scattering, typically requires more complex adaptive approaches to compensate [27]. Our results in Figs. 2–4 show that reducing scattering improves both imaging depth and image quality.

In summary, a novel imaging platform was demonstrated for studying subcortical regions noninvasively in living mice. Reduced scattering at 1.7 μm is shown to improve penetration depth compared to 1.3 μm. A future study will employ dynamic focusing to better characterize differences in vasculature and attenuation coefficients by cortical layer. Currently, the 1.7 μm system has a relatively low sensitivity (~91 dB with a sample incident power of 5 mW), mainly due to power loss caused by using off-the-shelf optics and the high noise of extended InGaAs cameras. Customized low-loss 1.7 μm anti-reflection-coated optics will help to alleviate the former problem. Further technical considerations to be addressed include sample heating and depth-dependent dispersion compensation.

Future work will include longitudinal studies of substrates associated with impaired memory in rodent models of Alzheimer's disease and subcortical dementias, including vascular dementias, as well as studies investigating mechanisms of neurovascular coupling in white matter.

REFERENCES

1. F. Helmchen and W. Denk, Nat. Methods **2**, 932 (2005).
2. P. Theer, M. T. Hasan, and W. Denk, Opt. Lett. **28**, 1022 (2003).
3. P. Theer and W. Denk, J. Opt. Soc. Am. A **23**, 3139 (2006).
4. R. K. Wang, S. L. Jacques, Z. Ma, S. Hurst, S. R. Hanson, and A. Gruber, Opt. Express **15**, 4083 (2007).
5. V. J. Srinivasan, H. Radhakrishnan, E. H. Lo, E. T. Mandeville, J. Y. Jiang, S. Barry, and A. E. Cable, Biomed. Opt. Express **3**, 612 (2012).
6. S. L. Jacques, Phys. Med. Biol. **58**, R37 (2013).
7. R. K. Wang and L. An, Opt. Express **17**, 8926 (2009).
8. D. Kobat, M. E. Durst, N. Nishimura, A. W. Wong, C. B. Schaffer, and C. Xu, Opt. Express **17**, 13354 (2009).
9. N. G. Horton, K. Wang, D. Kobat, C. G. Clark, F. W. Wise, C. B. Schaffer, and C. Xu, Nat. Photonics **7**, 205 (2013).
10. S. Ishida, N. Nishizawa, T. Ohta, and K. Itoh, Appl. Phys. Express **4**, 052501 (2011).
11. U. Sharma, E. W. Chang, and S. H. Yun, Opt. Express **16**, 19712 (2008).
12. E. J. Jung, J. H. Lee, B. S. Rho, M. J. Kim, S. H. Hwang, W.-J. Lee, J.-J. Song, M. Y. Jeong, and C.-S. Kim, IEEE J. Sel. Top. Quantum Electron. **18**, 1200 (2012).
13. S. Ishida and N. Nishizawa, Biomed. Opt. Express **3**, 282 (2012).
14. R. F. Reinoso, B. A. Telfer, and M. Rowland, J. Pharmacol. Toxicol. Methods **38**, 87 (1997).
15. S. Makita, T. Fabritius, and Y. Yasuno, Opt. Express **16**, 8406 (2008).
16. P. J. Drew, A. Y. Shih, J. D. Driscoll, P. M. Knutsen, P. Blinder, D. Davalos, K. Akassoglou, P. S. Tsai, and D. Kleinfeld, Nat. Methods **7**, 981 (2010).
17. S. P. Chong, C. W. Merkle, C. Leahy, H. Radhakrishnan, and V. J. Srinivasan, Biomed. Opt. Express **6**, 1429 (2015).
18. V. J. Srinivasan, H. Radhakrishnan, J. Y. Jiang, S. Barry, and A. E. Cable, Opt. Express **20**, 2220 (2012).
19. D. J. Faber, F. J. van der Meer, M. C. G. Aalders, and T. G. van Leeuwen, Opt. Express **12**, 4353 (2004).
20. S. L. Jacques, D. Levitz, R. Samatham, D. S. Gareau, N. Choudhury, and F. Truffer, in *Biomedical Applications of Light Scattering*, W. Adam and B. Vadim, eds. (McGraw-Hill, 2010), pp. 171–191.
21. F. Gallyas, Neurol. Res. **1**, 203 (1979).
22. S. W. Jeon, M. A. Shure, K. B. Baker, D. Huang, A. M. Rollins, A. Chahlavi, and A. R. Rezai, J. Neurosci. Methods **154**, 96 (2006).
23. P. Andersen, *The Hippocampus Book* (Oxford University, 2007).
24. R. K. Wang, Phys. Med. Biol. **47**, 2281 (2002).
25. M. J. Yadlowsky, J. M. Schmitt, and R. F. Bonner, Appl. Opt. **34**, 5699 (1995).
26. G. S. Hong, S. Diao, J. L. Chang, A. L. Antaris, C. X. Chen, B. Zhang, S. Zhao, D. N. Atochin, P. L. Huang, K. I. Andreasson, C. J. Kuo, and H. J. Dai, Nat. Photonics **8**, 723 (2014).
27. N. Ji, T. R. Sato, and E. Betzig, Proc. Natl. Acad. Sci. USA **109**, 22 (2012).